J Mater Sci (2010) 45:4021–4028
DOI 10.1007/s10853-010-4480-x

Phase characterization in as-cast F-75 Co–Cr–Mo–C alloy

R. Rosenthal · B. R. Cardoso · I. S. Bott · R. P. R. Paranhos · E. A. Carvalho

Received: 1 January 2010 / Accepted: 5 April 2010 / Published online: 29 April 2010

Abstract Microstructural characterization of a cast acetabulum of ASTM F-75 alloy has been carried out in order to clarify conflicting reports from the literature. The present investigation revealed that although sigma (σ) and $M_{23}C_6$ carbide were the only secondary phases formed in the face centered cubic cobalt-base alpha matrix (Co-α), as identified by X-ray diffraction, the observed microstructure was quite complex. Scanning and transmission electron microscopy indicated the presence of coarse and fine lamellar cellular colonies, grain boundary film carbide, and different types of coarse blocky particles, including single-phase σ, dual-phase $\sigma/M_{23}C_6$, a binary eutectic comprised of σ and Co-α phases, and a three-phase feature comprising the binary eutectic and solid state formed $M_{23}C_6$. The carbide has probably formed during cooling from casting due to σ metastability. While it is proposed that the some lamellar cellular colonies were formed by discontinuous precipitation, it is not clear whether all lamellar structures present in the as-cast alloy occurred due to the same mechanism. The results obtained for the tensile properties are discussed in view of the observed microstructure.

R. Rosenthal (✉) · R. P. R. Paranhos · E. A. Carvalho
Universidade Estadual do Norte Fluminense Darci Ribeiro, Advanced Materials Laboratory, Campos dos Goytacazes 28013-602, Brazil
e-mail: ruben@uenf.br

B. R. Cardoso
Centro de Pesquisas de Energia Elétrica, Rio de Janeiro 21941-911, Brazil

I. S. Bott
Department of Metallurgy and Materials Science, Pontifícia Universidade Católica do Rio de Janeiro, Rio de Janeiro 22453-900, Brazil

Introduction

Cobalt alloy investment casts are still widely exploited in the manufacturing of orthopedic implants, even with the advent of lighter titanium alloys, mainly when good wear properties are required, such as for hip joints [1, 2]. Hard blocky particles embedded in a high toughness matrix [2] provide superior wear properties in the as-cast material in comparison with the wrought condition. However, ductility of the as-cast alloy often failed to achieve the minimum requirement. Conflicting reports still exist concerning the microstructure of as-cast cobalt F-75 alloy [3] and its effects on the alloy properties [4].

The main reported secondary phases present in the dendrites of face centered cubic (fcc) Co-α matrix of the F-75 alloy are $M_{23}C_6$ carbide and σ phase. Most authors referred to the presence of large blocky particles in inter-dendritic regions, but while several works identified or mentioned such particles as carbides [4–11], mostly $M_{23}C_6$, others pointed to the sole presence of blocky σ phase particles [12], or to both carbide and σ [3, 13, 14] particles. Lamellar carbides [3, 9, 11–13] of reported eutectic [4] or eutectoid origin [5, 15] and grain boundary film carbide [5, 8, 13] have been observed at grain boundaries. It should be noted, however, that some of the phase characterization work reported in the literature relied mainly on stain etching, without the employment of diffraction or chemical microanalysis techniques.

It has been verified that the amount of blocky and lamellar carbides varied with the casting parameters (pouring and mold temperatures) [4, 5]. Ramirez et al. [3], using the technique of quenching during the directional solidification (QDS) of a F-75 alloy (0.26 wt% C), observed that σ phase formed at the end of the solidification range (around 1,200 °C), both as individual blocky

particles and as a binary eutectic with Co-α phase; further cooling led metastable σ to transform into $M_{23}C_6$ carbide at a temperature below 1,150 °C. Other QDS experiments conducted on F-75 alloys with carbon contents varying from 0.26 to 0.45 wt% indicated that only for the alloys with high carbon content (0.36 and 0.45 wt%), could a thermal peak at the cooling rate curves be associated with $M_{23}C_6$ carbide formation from σ [15]. The formation of lamellar "eutectoid" carbides occurred for cooling rates varying from 8 to 16 °C/min, in fair agreement with previous results [3] that verified that the maximum cooling rate for the formation of lamellar cellular colonies as 35 °C/min. The lamellar structure formed during cooling at temperatures under 990 °C [3], thus after solidification was complete. The amount of both blocky [15] and lamellar [11, 15] carbides was found to increase with carbon content.

The tensile properties requirements, as specified by the ASTM F-75 standard, are 655 MPa ultimate tensile limit (UTS), 450 MPa yield strength (YS), and 8% elongation (Є). Strengthening of as-cast Co–Cr–Mo–C alloys is mainly due to solid solution strengthening [16] and by dislocation interactions with stacking fault intersections [17]. The coarse blocky carbides also play an important role, acting both as excellent sources of dislocations and stacking faults under the influence of stresses [14, 16] and as elastic inclusions to reinforce the matrix, thus increasing the YS in proportion to the volume fraction of particles [18]. For strains higher than 0.01–0.02, extensive cracking of carbide particles would lead to flow stress control by dislocation–dislocation or dislocation–solute interactions [18].

Concerning ductility, there are only few reports where the minimum elongation requirement was achieved for the as-cast alloy. Asgar and Peyton [5] obtained elongation values up to 12%, but it has been suggested [4] that errors could have been introduced due to the use of non-standard gauge length specimens. While Cohen et al. [14] reported values as high as 15% elongation, no microstructural evaluation was presented in order to explain their results. Zhuang and Langer [19] obtained 11.8% elongation, plus superior YS and UTS values, when a metallic mold coupled with water cooling was used for achieving a fast cooling rate, which resulted in fine equiaxed grain structure. Also, as a result of cooling conditions, the interdendritic coarse blocky carbide structure was replaced by a grain boundary necklace precipitation of fine particles; the effect of such microstructure on wear properties had not been examined by the authors.

The often reported failure of the as-cast alloy to achieve the required minimum ductility has been attributed to the combined effect of microporosity and unsuitable microstructure, such as lamellar carbides [4, 5] and continuous carbide films [5] at grain boundaries. However, despite minimizing the amount of lamellar colonies in porosity-free alloys by controlling the casting parameters [4, 5] or by lowering the carbon content [11], the ductility improvement was not significant. A satisfactory value could only be achieved after a solution heat treatment was applied to a porosity-free medium carbon alloy, drastically reducing the total amount of carbides [4, 11]. The UTS level had not been impaired by the reduction in the carbide fraction, as the increased amount of carbon in solution enhanced the contribution of intrinsic stacking faults to the alloy strengthening [11].

Information concerning the effect of blocky σ phase on the mechanical properties of σ-forming alloys is scarce in literature. If present in a plate-like or angular morphology, brittle σ phase particles are usually believed to decrease ductility as they provide preferential sites for crack initiation and growth [20]. It has been suggested that the massive blocky morphology might not be particularly detrimental to properties [16]. Intragranular blocky σ particles, similar to the carbide particles, generate stacking faults during quenching [14] and thereby contribute to strengthening in the cobalt alloy. However, it has been otherwise reported [21] that blocky-type σ particles, together with $M_{23}C_6$ carbides, were associated with the reduction in room temperature tensile elongation for a σ-containing alloy. Furthermore, for AISI type 316 stainless steel containing both σ and $M_{23}C_6$ blocky particles, crack formation and propagation clearly occurred at a lower deformation level in σ phase [22]. The presence of an interdendritic σ/fcc cobalt-rich/$M_{23}C_6$ eutectic was associated to a reduction in ductility to fracture in F-75 alloy [18].

The present work was carried out as an attempt to improve the phase characterization of an as-cast Co–Cr–Mo–C alloy and contribute to the achievement of a better understanding of the effect of microstructure on mechanical properties.

Experimental procedure

This investigation was carried out on both a cast acetabulum and on cast-to-size test pieces for tensile tests, supplied by the manufacturer, with nominal composition (wt%) Co–28Cr–6Mo–0.25C. Casting parameters were 1,620 °C for the metal pouring temperature, and 1,000 °C for the mold temperature. Hot isostatic pressing (HIP) processing was not applied. Tensile tests were performed in accordance with ASTM E-8 procedures on specimens of 6 mm diameter at the gauge region.

The microstructural investigation included optical microscopy (OM), scanning electron microscopy (SEM) coupled with energy dispersive spectrometry (EDS) microanalysis

of both bulk metallic pieces and electrolytically extracted particles, X-ray diffraction (XRD) of extracted particles and electron diffraction (ED) of thin-foil specimens in the transmission electron microscope (TEM). For OM and SEM examination, the sample surface received final polishing with 0.1 μm size alumina prior to electrolytic etching with a citric acid–ammonium sulfate based solution that preferentially dissolved the cobalt-base matrix. Particle extraction for XRD, SEM, and EDS examination was performed using an HCl–methanol electrolyte. Electron-transparent thin-foil specimens for TEM examination were prepared by jet polishing in a perchloric acid–ethanol solution.

Results and discussion

Microstructural examination by optical microscopy showed a dendritic solidification pattern (Fig. 1) and the presence of grain boundary and interdendritic features. The casting parameters led to the formation of microporosity despite the high pouring temperature. The identification of the secondary phases present in the matrix was initially carried out using XRD analysis of extracted particles (Fig. 2), which revealed the presence of $(CrCoMo)_{23}C_6$ carbide (in agreement with Youdelis and Kwon [7]) and prominent diffraction lines confirming the presence of σ phase. The lattice parameter of the carbide as obtained from XRD analysis is 10.81 Å. σ phase was identified after comparison of the present XRD results with data available for (CrCo) σ. Some observed differences in peak intensity, when comparing both data, may be attributed to the verified Mo content (approximately 20 wt%) in the σ composition for the F-75 alloy. The lattice parameters obtained from XRD analysis for the tetragonal structure are 8.84 and 4.53 Å.

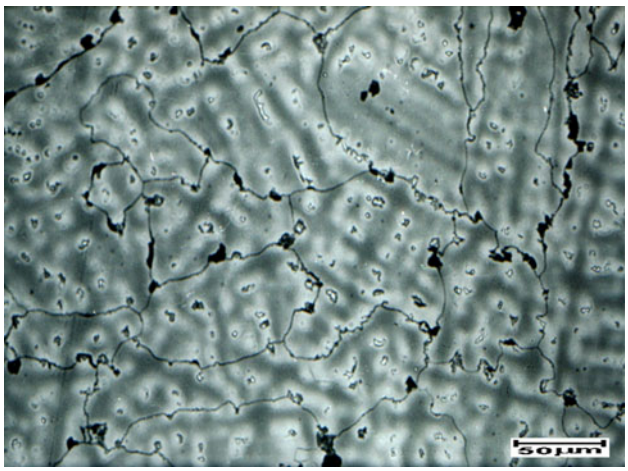

Fig. 1 As-cast microstructure showing features at grain boundaries and interdendritic regions (optical micrograph)

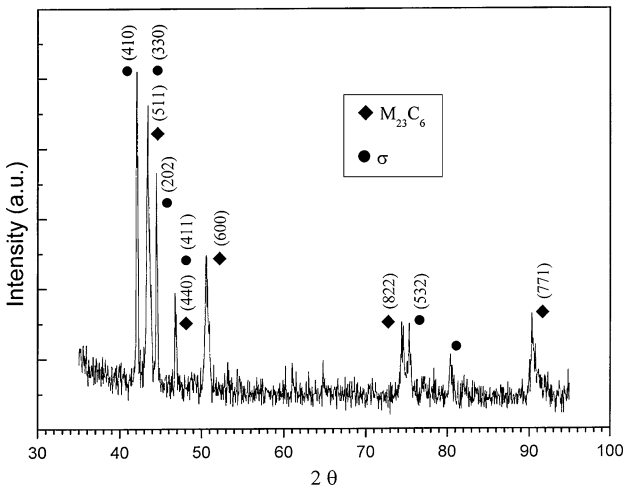

Fig. 2 X-ray diffraction analysis of extracted particles of the as-cast material

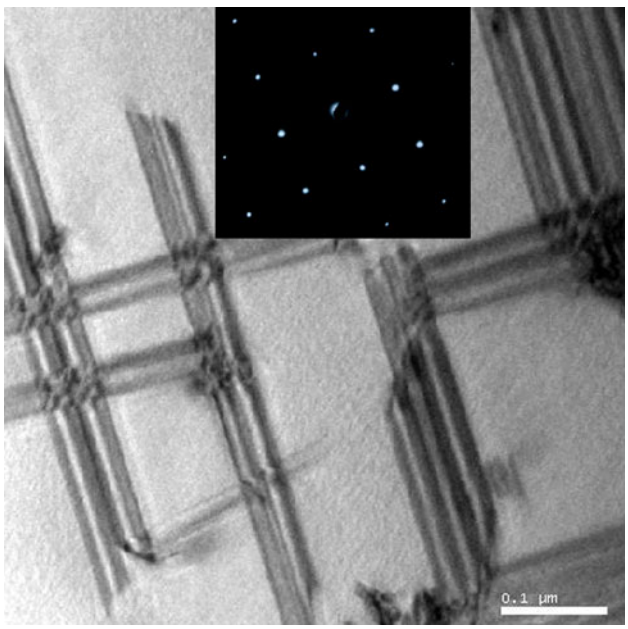

Fig. 3 Intersecting stacking fault bands (TEM micrograph) and [100] zone axis selected area electron diffraction pattern for Co-α matrix

TEM examination of the fcc Co-α matrix revealed the presence of numerous stacking faults (Fig. 3), as expected; the lattice parameter for the matrix, as obtained from the [100] oriented ED pattern, is 3.66 Å.

The SEM examination of the secondary phases revealed the presence of a complex microstructure at the interdendritic regions, including blocky particles, lamellar cellular colonies, a *quasi-continuous* grain boundary film and a dispersion of silicon-rich spherical inclusions.

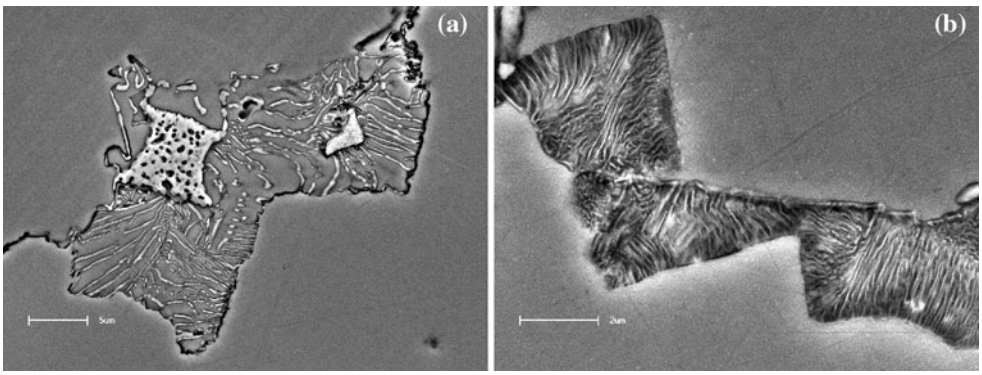

Fig. 4 Lamellar cellular colonies at grain boundaries: **a** coarse lamellae and blocky particles, **b** fine lamellae (SEM micrographs)

In Fig. 4, coarse and fine lamellae comprising cellular colonies formed at grain boundaries are shown, respectively. Some lamellae are curved in accordance with variations in their growth direction following changes in the migration direction of the moving front. The overall morphology of the lamellar colonies for both cases suggests a possible growth by grain boundary movement, as occurs for discontinuous (cellular) reactions, whereby the coupled lamellae growth is controlled by grain boundary diffusion [23]. There are previous reports of discontinuous phase formation during cooling from casting for other alloy systems [24]. This mechanism has not been previously proposed to explain the lamellar formation in as-cast F-75 alloy. The only reported presence of discontinuous lamellar cellular colonies in a Co–Cr–Mo–C alloy referred to the alloy aged in the range of 650 to 900 °C [25]. Based on TEM and microprobe analysis, Kilner et al. [12] have reported that the cellular colonies they observed consisted of alternate lamellae of $M_{23}C_6$ and fcc cobalt-rich matrix. Their result is consistent with the reported lamellar carbide formation during continuous cooling at around 990 °C [3, 15] after solidification was complete. This is also a temperature at which σ is metastable in F-75 alloy [3, 15], thus favoring preferential $M_{23}C_6$ formation. However, for some of the fine lamellae cellular colonies that were observed both at grain boundaries and at adjacent regions (Fig. 5), further investigation is required in order to establish their formation mechanism, since there is no clear evidence at the present work to suggest that they have grown by a discontinuous reaction. These colonies may have otherwise originated from eutectoid precipitation, a mechanism that has already been proposed [5, 15] to explain the lamellar formation in F-75 alloy.

Figure 6 is an SEM micrograph showing an interdendritic light-gray blocky phase and a silicon-rich spherical inclusion, as determined using EDS microanalysis. The light-gray phase was also characterized using TEM, as shown in Fig. 7 (region on the left side of the photograph). The electron diffraction pattern obtained is in accordance with a [213] zone axis for the tetragonal σ phase. In the SEM micrograph of Fig. 8, cavities (dark-gray regions) are observed in a light-gray blocky particle; these cavities resulted from preferential phase dissolution during the selective etching procedure. A similar etching effect also occurred in the Co-α matrix, thus suggesting the presence of Co-α phase in the interior of some σ

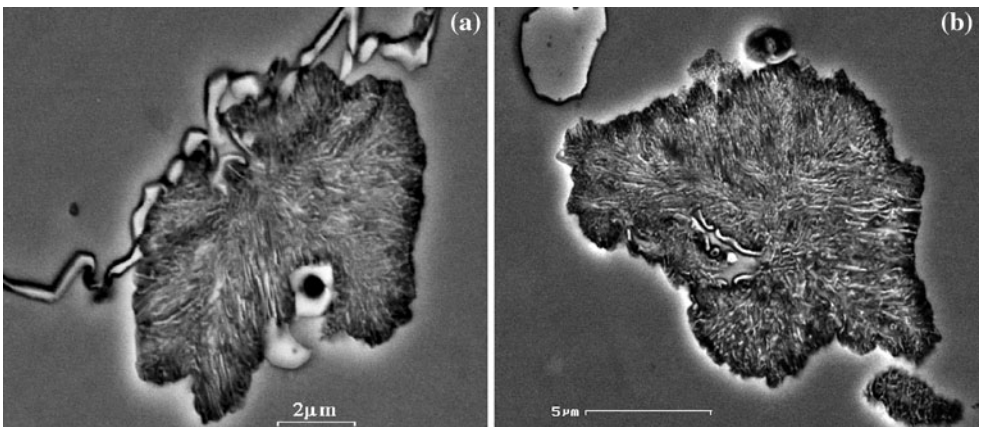

Fig. 5 Fine lamellae cellular colonies: **a** location at grain boundary, **b** location away from the grain boundary (SEM micrographs)

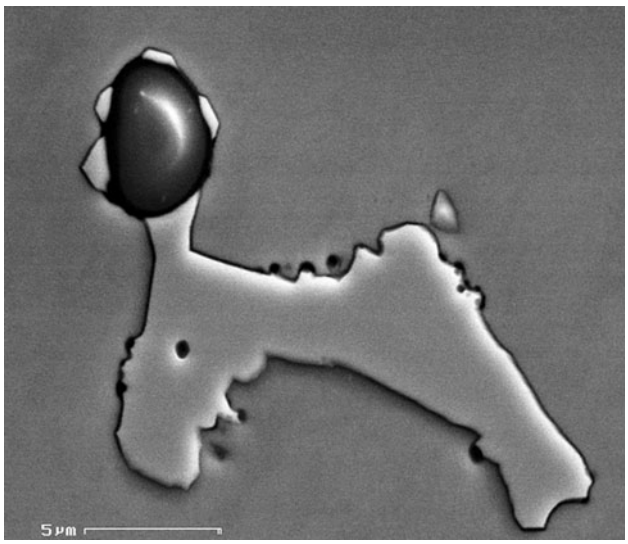

Fig. 6 Blocky σ particle and spherical silicon-rich inclusion (SEM micrograph)

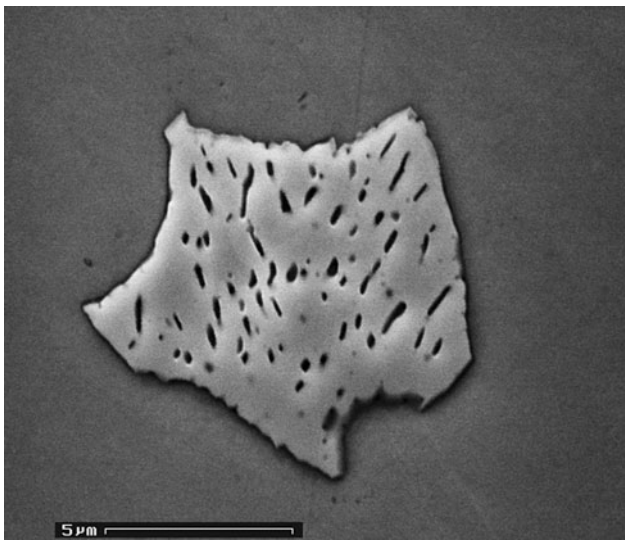

Fig. 8 Particle of apparent eutectic origin comprised blocky σ and Co-α globules and rods at the inside (SEM micrograph)

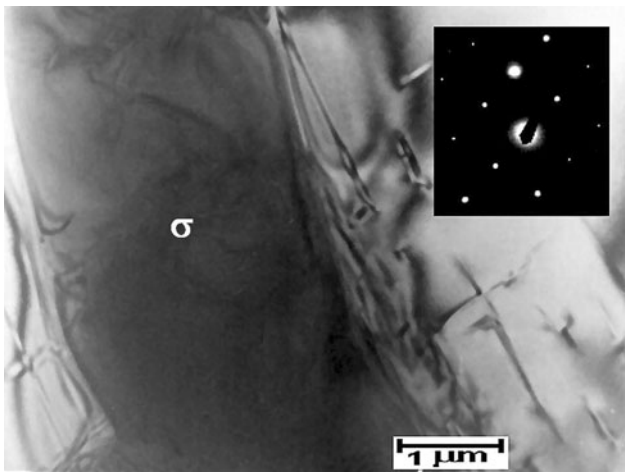

Fig. 7 TEM micrograph and [213] zone axis selected area electron diffraction pattern for σ phase

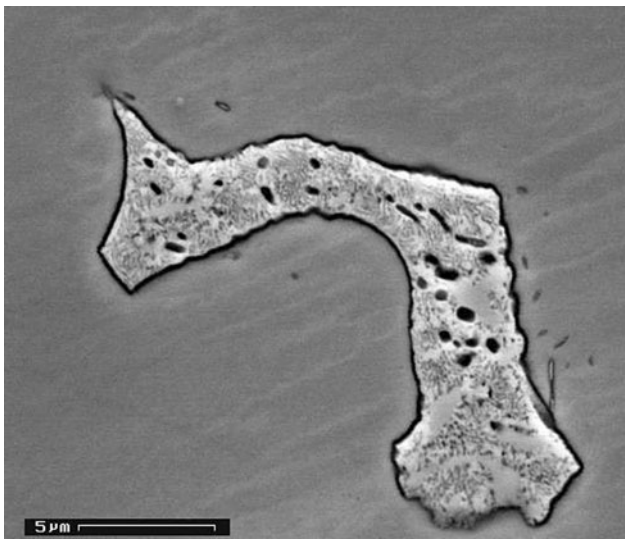

Fig. 9 Three-phase particle consisting of blocky σ, Co-α globules, and very fine $M_{23}C_6$ carbides (SEM micrograph)

particles. A previous proposition based on the QDS experiment [3] stated that σ phase was observed both as individual particles and as part of a binary eutectic with Co-α phase. Thus, Fig. 8 is consistent with that proposed σ/Co-α eutectic.

In Fig. 9 (SEM micrograph), a fine submicron structure can also be observed in a σ/Co-α "eutectic" particle, indicating that a third phase is present. This phase had also been observed in some of the blocky σ particles in the absence of Co-α phase. TEM characterization revealed that the additional phase was $M_{23}C_6$ (Fig. 10). The corresponding electron diffraction pattern is oriented according to the [111] direction. The lattice parameter obtained from the analysis of the diffraction pattern is 11.15 Å, thus in fair agreement with the value obtained from XRD (10.81 Å). The observed interference fringes in Fig. 10 are due to the overlapping of nano-size $M_{23}C_6$ carbides. As reported in the QDS experiment [3, 15], the $M_{23}C_6$ carbides formed from metastable σ phase during cooling following the alloy solidification.

The examination of electrolytically extracted particles in the SEM brought a further understanding of carbide formation from blocky σ particles. In Fig. 11, two distinct regions of the particle can be observed, viz., a *sponge-like* shell and an inner, massive core. This feature appears to consist of a σ phase core and an outer layer comprised $M_{23}C_6$ carbides, and would result from a partial $\sigma + C \Rightarrow M_{23}C_6$ reaction during cooling. For small σ

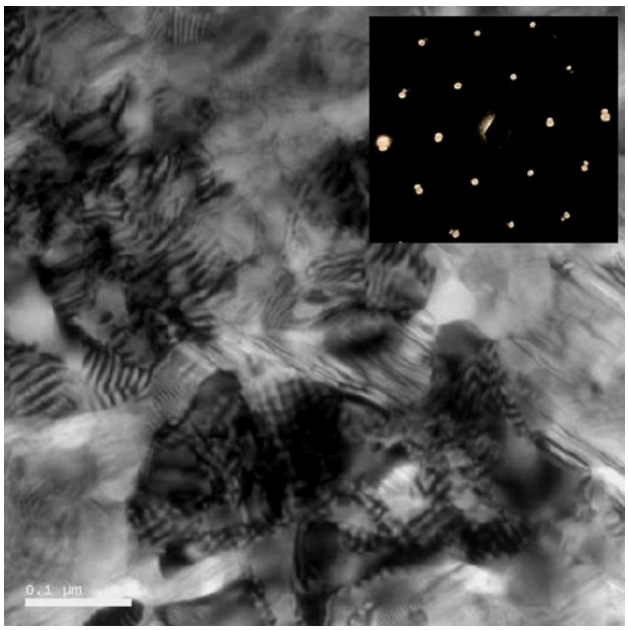

Fig. 10 TEM micrograph showing nano-size grain structure and [111] zone axis selected area electron diffraction pattern for $M_{23}C_6$

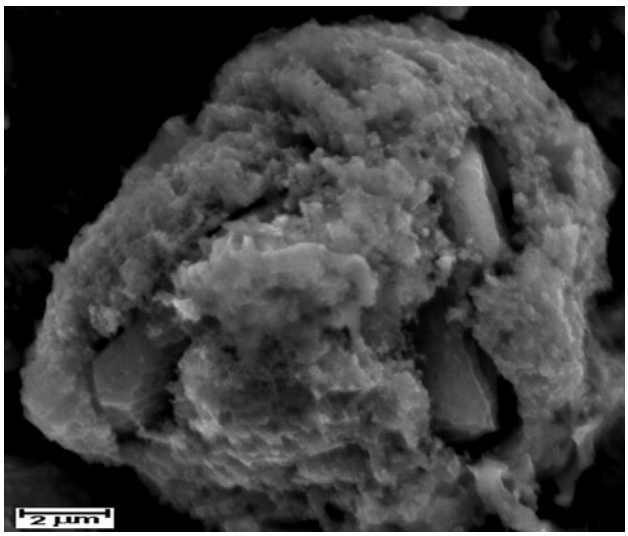

Fig. 11 Extracted blocky particle revealing an inner core and an *spongy* external shell, identified as σ phase and $M_{23}C_6$, respectively (SEM micrograph)

particles full transformation into $M_{23}C_6$ may have occurred. Digital EDS compositional maps obtained from extracted particles (Fig. 12) indicated that the core of the particle (σ region) is richer in Mo and has less Co than the carbide shell. Spot EDS analysis has shown that the approximate metal content (wt%) at the core and shell regions are 43Cr–38Co–19Mo and 34Cr–56Co–10Mo, respectively. The presence of molybdenum in the σ phase in σ-prone Mo-containing alloys is not unusual, and probably explains the small differences in the XRD pattern obtained from σ phase for the F-75 alloy (Fig. 2) when comparing it with standard data from (CoCr) σ.

Based on the XRD data for the as-cast condition, the amount of σ phase for the present alloy is significantly higher than reported for other studies in the literature where σ has formed in the F-75 alloy [3]. Minor variations in the alloy composition and differences in the casting parameters might explain the different reports about the alloy microstructure concerning the formation of sigma phase.

The results obtained for the tensile properties were 680 MPa UTS, 284 MPa YS, and 4.9 % ϵ; thus, neither yield strength nor elongation achieved the minimum requirement. The work hardening rate depends mainly on the volume fraction and elastic modulus of the coarse carbide particles that reinforce the matrix [18], provided that the particles do not crack. As blocky σ was reported [22] to favor crack formation, the presence of single-phase σ, $\sigma/M_{23}C_6$, σ/Co-α, and σ/Co-$\alpha/M_{23}C_6$ blocky particles in the present alloy might explain the low yield strength as compared to an F-75 alloy containing only blocky carbide particles. For high strains, extensive carbide crack formation occurs then interlocking stacking faults present in the fcc matrix control work hardening and flow stress [18], resulting in a satisfactory UTS value for the present alloy, as both $M_{23}C_6$ and σ can act as sources of stacking faults [14, 16]. The low value obtained for elongation is not unexpected due to the presence of microporosity. Furthermore, from previous results [18, 22], it should also be expected that a microstructure containing a distribution of blocky $M_{23}C_6$ and σ phase containing particles, rather than just $M_{23}C_6$ carbides, would result in inferior ductility. However, the present elongation data, although below the required value, are slightly above several results reported in the literature, even some that were obtained from porosity-free alloys [4, 11]. This indicates that other microstructural characteristics such as grain size, the formation of continuous film carbide at grain boundaries as opposed to a chain of particles, and the volume fraction of the lamellar cellular colonies and blocky particles have also to be considered in order to explain the elongation behavior of alloys cast under different conditions.

Conclusions

The characterization of the F-75 acetabulum by X-ray diffraction revealed that the amount of σ phase formed in the as-cast alloy was quite significant. Different types of blocky particles formed in the interdendritic regions of the fcc Co-α matrix included single-phase σ, two-phase $\sigma/M_{23}C_6$, σ/Co-α eutectic, and three-phase σ/Co-$\alpha/M_{23}C_6$ particles. The carbide formed due to σ metastability during

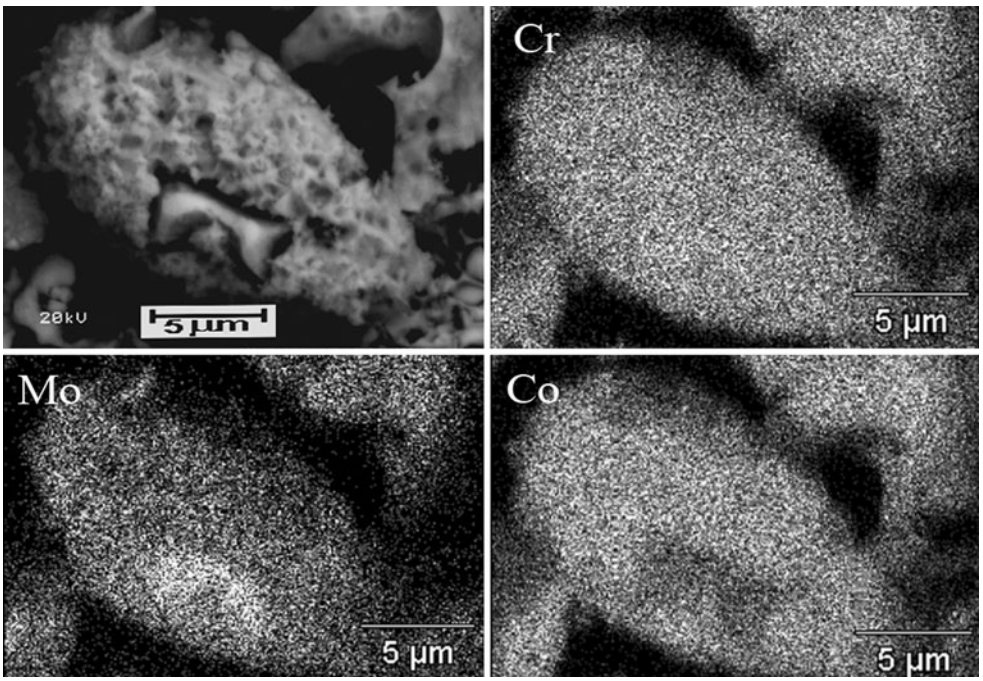

Fig. 12 EDS X-ray maps of an extracted blocky particle, showing a σ core richer in Mo and poorer in Co

cooling from casting, giving rise to a nano-scale grain structure forming a shell around a σ core, as the $\sigma \Rightarrow M_{23}C_6$ reaction was only partial for large σ particles. For small σ particles, full transformation into $M_{23}C_6$ may have occurred. A quasi-continuous film carbide was present at grain boundaries. Coarse and fine cellular colonies of lamellar carbide also formed at grain boundaries or adjacent regions. A discontinuous reaction mechanism is proposed for the formation of coarse and some of the fine cellular colonies.

As for the mechanical properties, the formation of single-phase σ and σ-containing blocky particles might explain the low level achieved for the yield strength. A satisfactory value was obtained for UTS, as it is likely that all blocky particles would contribute to the formation of stacking faults, which are responsible for the strengthening at high strains. As for the low observed ductility, the presence of porosity and the formation of σ phase would have reduced the elongation. However, the volume fraction of the lamellar cellular colonies and blocky particles, grain size, and the formation of a continuous carbide film at grain boundaries are also expected to play a role, which should be considered in any attempts to improve ductility in the F-75 alloy. Optimization of carbon content and casting parameters can probably provide such improvement for the as-cast alloy.

Acknowledgements R. Rosenthal wishes to acknowledge a grant received from the National Research Council (CNPq) of Brazil.

References

1. Davis JR (2003) Handbook of materials for medical devices. ASM International, Materials Park, OH
2. Marti A (2000) Injury 31:18
3. Ramírez LE, Castro M, Méndez M, Lacaze J, Herrera M, Lesoult G (2002) Scr Mater 47:811
4. Gómez M, Mancha H, Salinas A, Rodríguez JL, Escobedo J, Castro M, Mendez M (1997) J Biomed Mater Res 34:157
5. Asgar K, Peyton P (1961) J Dent Res 40:63
6. Clemow AJT, Daniell BL (1979) J Biomed Mater Res 13:265
7. Youdelis WV, Kwon O (1983) Met Sci 17:379
8. Ocampo CM, Talavera M, Lopez H (1999) Metall Mater Trans A 30:611
9. Mancha H, Carranza E, Escalante JI, Mendoza G, Méndez M, Cepeda F, Valdés E (2001) Metall Mater Trans A 32:979
10. De la Garza Z, Herrera-Trejero M, Castro MR, Ramirez ER, Méndez MN, Méndez J (2001) J Mater Eng Perform 10(2):153
11. Herrera M, Espinoza A, Méndez J, Castro M, López J, Rendón JN (2005) J Mater Sci Mater Med 16:607
12. Kilner T, Pilliar RM, Weatherly GC, Allibert C (1982) J Biomed Mater Res 16:63
13. Caudillo M, Herrera-Trejo M, Castro MR, Ramírez E, González CR, Juarez JI (2002) J Biomed Mater Res 59:378
14. Cohen J, Rose RM, Wulff J (1978) J Biomed Mater Res 12(4):935
15. Ramírez-Vidaurri LE, Castro-Román M, Herrera-Trejo M, García-Lopez CV, Almanza-Casas E (2009) J Mater Process Technol 209:1681
16. Sims CT (1972) In: Hagel WC, Sims CT (eds) The superalloys. Willey, New York
17. Rajan K, Vander Sande JB (1982) J Mater Sci 17:769. doi: 10.1007/BF00540374
18. Kilner T, Laanemae WL, Pilliar RR, Weatherly GC, MacEwen SR (1986) J Mater Sci 21:1349. doi:10.1007/BF00553274

19. Zhuang LZ, Langer EW (1989) J Mater Sci 24:381. doi:10.1007/BF01107415
20. Charre MD (1997) The microstructure of superalloys. Gordon and Breach Sci Publ, New York
21. Tawancy HM (1983) J Mater Sci 18:2976. doi:10.1007/BF00700780
22. Senior BA (1990) J Mater Sci 25:45. doi:10.1007/BF00544182
23. Williams DB, Butler EP (1981) Int Mater Rev 26:153
24. Rosenthal R, West DRF (1986) Mater Sci Tecnol 2:169
25. Taylor RNJ, Waterhouse RB (1983) J Mater Sci 18:3265. doi:10.1007/BF00544151